Synchronous and Asynchronous Chaos in Coupled Neuromodules *

Frank Pasemann
Max-Planck-Institute for Mathematics in the Sciences
Inselstr. 22-26, D-04103 Leipzig, Germany
email: f.pasemann@mis.mpg.de

Abstract

The parametrized time-discrete dynamics of two recurrently coupled neuromodules is studied analytically and by computer simulations. Conditions for the existence of synchronized dynamics are derived and periodic as well as quasiperiodic and chaotic attractors constrained to a synchronization manifold M are observed. Stability properties of the synchronized dynamics is discussed by using Lyapunov exponents parallel and transversal to the synchronization manifold. Simulation results are presented for selected sets of parameters. It is observed that locally stable synchronous dynamics often co-exists with asynchronous periodic, quasiperiodic or even chaotic attractors.

*published in: *International Journal of Bifurcation and Chaos*, **9**, 1957–1968 (1999).

1 Introduction

Ever since the feasibility of synchronizing chaotic systems has been established also by Pecora & Carroll [1990], this phenomenon has been investigated in many articles. Part of the work on synchronized chaos has been motivated by its potential for technical applications (e.g. [Parlitz *et al.*, 1992; Cuomo & Oppenheimer, 1993; Kapitaniak *et al.*, 1996]). But still there is an ongoing discussion of its various theoretical aspects [Kocarev *et al.*, 1993; Heagy *et al.*, 1994; Schweizer *et al.*, 1995; Rulkov *et al.*, 1995; Rosenblum *et al.*, 1996; Pikovsky *et al.*, 1997; Hasler *et al.*, 1998; Astakhov *et al.*, 1998]. The coupling of time-continuous systems - like Chua's circuit, or Lorenz or Rössler systems - has been studied, as well as the coupling of time-discrete systems, as is examined in this article (e.g. [De Sousa Viera *et al.*, 1992; Maistrenko & Kapitaniak, 1996; Astakhov *et al.*, 1998]). Synchronized chaotic dynamics has been observed and analyzed for one-way couplings, but also for recurrent couplings, where each of the subsystems effects the other. The latter case is discussed in this article.

Selective synchronization of neural activity in biological brains, on the other hand, has often been suggested to be a fundamental temporal mechanism for binding spatially distributed features into a coherent object (cf. e.g. [Eckhorn *et al.*, 1988; Singer, 1994; Engel *et al.*, 1997]). In this context conceptual discussions and biologically motivated models were mainly based on partial synchronization of oscillatory dynamics in large, e.g. high-dimensional systems [Carroll, 1995; Hansel & Sompolinsky, 1992; Pecora *et al.*, 1994; Wennekers & Pasemann, 1996]. But with respect to brain theory and neural network modelling it seems that one is often not aware of the rich phenomenology displayed by coupled nonlinear systems.

On this background we will present some examples of the dynamical phenomena observed for the time-discrete dynamics of two recurrently coupled neural networks. These networks are supposed to have only few neurons, and because they are considered as basic building blocks for larger systems, they are termed 'neuromodules'. In the following they are described as low-dimensional parametrized dynamical systems with nonlinearities introduced by the sigmoidal transfer functions of additive neurons. As parameters we will consider bias terms and/or stationary inputs, the synaptic strengths or weights between module neurons and the coupling strength between modules. Thus, the neuromodules are treated here as a general type of neural networks with no conditions on the weights (e.g. no symmetry conditions). Different from 'classical' neural networks - like feedforward networks or Hopfield networks (cf. e.g. [Hertz *et al.*, 1991]), which have convergent dynamics - these systems are allowed to have periodic as well as chaotic dynamics.

We will use the term 'synchronization' in the sense of *complete synchronization*; i.e. the states of the systems will coincide, while the dynamics in time remains periodic or chaotic. We will also discern between global and local syn-

chronization. Global synchronization describes a situation, where for almost all initial conditions the orbits of the systems will synchronize. By local synchronization we refer to asymptotically stable synchronized states; i.e. small perturbations will not de-synchronize the systems. This is often also called 'strong synchronization'.

In Sec. 2 general conditions for the existence of synchronized dynamics of coupled neuromodules are derived. These conditions show that the individual modules, having the same number of neurons, do not have to be identical to achieve synchronous behavior; in fact, they may have different weights; i.e. they represent different dynamical systems of the same dimension. Different weights are then 'compensated' by corresponding asymmetric couplings. This defines a slightly more general setup for the discussion of synchronous chaos where usually symmetric couplings are assumed (cf. for instance [Astakhov *et al.*, 1998]). Furthermore, in general analytical treatments use linear couplings (e.g. [Maistrenko & Kapitaniak, 1996]); but in the neural network context we canonically have to deal with the nonlinear coupling of subsystems. This makes analytical statements on the stability conditions for the synchronous dynamics much more difficult to achieve.

The stability properties of a synchronous dynamics in coupled neuromodules is discussed along well established lines [Venkataramani *et al.*, 1996; Ashwin *et al.*, 1996]: A *synchronization manifold* M is introduced together with its *synchronization* and *transversal Lyapunov exponents*. Synchronized chaos will be characterized by at least one positive synchronization exponent; unstable synchronized dynamics by at least one positive transversal exponent. Thus, unstable synchronized chaos will always be associated with hyperchaotic systems, i.e. with systems having at least two positive Lyapunov exponents [Rössler, 1979].

In Sec. 3 we present numerical examples for the dynamics of 2-neuron modules, which can be understood as remnants of the Cowan-Wilson model of excitatory and inhibitory neuron interaction [Wilson & Cowan, 1972]. The dynamical behavior of the 2-neuron module is well known for large parameter domains [Wang, 1991; Blum & Wang, 1992; Chapeau-Blondeau & Chauvet, 1992; Pasemann, 1995a]. The first example in Sec. 3 studies coupled 2-neuron modules which operate in a chaotic regime when isolated. Here stable as well as unstable synchronized chaos is observed for different parameter domains. In the second example the coupled 2-neuron modules can have only global fixed point attractors or period-4 attractors if isolated [Pasemann, 1995b]. The chosen coupling of these modules results in synchronized chaos which is unstable whenever it appears; i.e. the only stable synchronous dynamics of the coupled system will be periodic. If there exist synchronous chaotic orbits, then the system will be hyperchaotic.

There is one more observation which should be emphasized in the context of neural network modelling: For large parameter domains synchronous dynamics of coupled neuromodules is only locally stable; i.e. together with synchronous periodic, quasiperiodic or chaotic attractors constrained to the synchronization

manifold M there co-exist asynchronous periodic, quasiperiodic or chaotic attractors in other parts of the phase space. In Sec. 4 a short summary of the results is given.

2 Coupled Neuromodules

We are considering neuromodules as discrete parametrized dynamical systems on an n-dimensional activity phase space $\mathbf{R}^n$ given by the map

$$a_i(t+1) = \theta_i + \sum_{j=1}^{n} w_{ij}\, \sigma(a_j(t)) \;, \quad i = 1, \ldots, n \;, \tag{1}$$

where $a_i \in \mathbf{R}^n$ denotes the activity of the i-th neuron, and $\theta_i = \overline{\theta}_i + I_i$ denotes the sum of its fixed bias term $\overline{\theta}_i$ and its stationary external input I_i, respectively. The output $o_i = \sigma(a_i)$ of a unit is given by the sigmoidal transfer function

$$\sigma(a) := \frac{1}{(1+e^{-a})} \;, \quad a \in \mathbf{R} \;, \tag{2}$$

and w_{ij} denotes the synaptic weight from unit j to unit i. A neuromodule having a parameter set $\rho = (\theta, w)$ for which the dynamics (1) has at least one chaotic attractor will be called a *chaotic neuromodule*. Note that neuromodules must not be completely connected; i.e., some w_{ij} may satisfy $w_{ij} = 0$. Furthermore, there are no special conditions for the weights $w_{ij} \neq 0$. Thus, self-connections w_{ii} are allowed and, for instance, symmetry conditions for weights, as is postulated by the theory of Hopfield networks [Hertz *et al.*, 1991] must not hold in the following.

Suppose A and B denote two chaotic neuromodules, each having n neurons with an architecture described by the nonzero elements of the $(n \times n)$-matrices w^A and w^B, respectively. Connections going from module B to module A are comprised in a $(n \times n)$ coupling matrix w^{AB}. Correspondingly, connections from module A to module B are given as a $(n \times n)$ coupling matrix w^{BA}. Thus, the architecture of the coupled system is given by a matrix w of the form

$$w = \begin{pmatrix} w^A & w^{AB} \\ w^{BA} & w^B \end{pmatrix} . \tag{3}$$

The neuronal activities of module A and B will be denoted a_i, b_i, $i = 1, ...n$, respectively. The activity phase space of the coupled system is of course $2n$-dimensional, and its discrete parametrized dynamics will be denoted by $F_\rho : \mathbf{R}^{2n} \to \mathbf{R}^{2n}$. Here $\rho := (\rho^A,\ \rho^B,\ w^{AB},\ w^{BA})$ denotes a set of parameters for the coupled system and $\rho^A := (\theta^A,\ w^A)$ is the parameter set of module A.

We will be interested mainly in the process of *complete synchronization* of module neurons, by which we mean that there exists a subset $D \subset \mathbf{R}^{2n}$ such that $(a_0, b_0) \in D$ implies

$$\lim_{t\to\infty} \mid a(t; a_0) - b(t; b_0) \mid = 0 \;,$$

where $(a(t;a_0), b(t;b_0))$ denotes the orbit under F_ρ through the initial condition $(a_0, b_0) \in \mathbf{R}^{2n}$. Thus we are interested in the case where corresponding neurons of the modules have identical activities during a process. The synchronization is called *global* if $D \equiv \mathbf{R}^{2n}$, and *local* if $D \subset \mathbf{R}^{2n}$ is a proper subset. Thus, a *synchronized state* s of the coupled system is defined by $s := a = b \in \mathbf{R}^n$. Correspondingly, a state $\hat{s}$ satisfying $\hat{s} = a = -b$ is called *anti-synchronized*. The *synchronization manifold* $M := \{(s,s) \in \mathbf{R}^{2n} \mid s = a = b\}$ of synchronized states corresponds to an n-dimensional hyperplane $M \cong \mathbf{R}^n \subset \mathbf{R}^{2n}$. We introduce coordinates parallel and orthogonal to the synchronization manifold M as follows:

$$\xi_i := \frac{1}{\sqrt{2}}(a_i + b_i) \quad , \quad \eta_i := \frac{1}{\sqrt{2}}(a_i - b_i) \; , \quad i = 1, \ldots, n \; . \tag{4}$$

Setting $\eta(t_0) = a(t_0) - b(t_0)) = 0$ for some t_0 we can immediately verify the following lemma by direct calculation.

Lemma 1 *Let the parameter sets ρ^A, ρ^B of the modules A and B satisfy*

$$\theta = \theta^A = \theta^B \; , \quad (w^A - w^{BA}) = (w^B - w^{AB}) \; . \tag{5}$$

Then M is an invariant manifold for the dynamics F_ρ.

This lemma applies to different special situations; for instance, to the case $w^{AB} = 0$, where module B is driven by module A. For simplicity, we will discuss in the following the symmetric coupling of identical modules, i.e. the parameter set $\rho = (\theta, w, w^{coup})$ satisfies

$$\theta := \theta^A = \theta^B \; , \quad w := w^A = w^B \; , \quad w^{coup} := w^{BA} = w^{AB} \; . \tag{6}$$

With respect to the synchronized dynamics in M there will be no qualitative differences to the general situation (5). The difference is mainly for the asynchronous dynamics, where under the general conditions (5) attractors will not lie symmetrically to the synchronization manifold M any longer.

2.1 Identical modules with symmetric couplings

Let $\rho = (\theta, w, w^{coup})$ denote a set of parameters satisfying condition (6). Using (ξ, η)-coordinates given by (4) the dynamics $\tilde{F}_\rho$ of two coupled identical modules is then given by

$$\begin{aligned} \xi_i(t+1) &= \sqrt{2} \cdot \theta_i + \frac{1}{\sqrt{2}} \sum_{j=1}^{2} w_{ij}^{+} \cdot G^{+}(\xi_j(t), \eta_j(t)) \; , \quad i = 1, \ldots, n \; , \\ \eta_i(t+1) &= \frac{1}{\sqrt{2}} \sum_{j=1}^{2} w_{ij}^{-} \cdot G^{-}(\xi_j(t), \eta_j(t)) \; , \quad i = 1, \ldots, n \; . \end{aligned} \tag{7}$$

where we have set

$$w^+ := (w + w^{coup}) \quad , \quad w^- := (w - w^{coup}) \; , \tag{8}$$

and the functions G^+, $G^- : \mathbf{R}^2 \to \mathbf{R}$ are defined by

$$\begin{aligned} G^+(x,y) &:= \sigma(\frac{1}{\sqrt{2}}\,(x+y)) + \sigma(\frac{1}{\sqrt{2}}\,(x-y)) \; , \\ G^-(x,y) &:= \sigma(\frac{1}{\sqrt{2}}\,(x+y)) - \sigma(\frac{1}{\sqrt{2}}\,(x-y)) \; . \end{aligned} \tag{9}$$

These functions have the following properties:

$$G^+(x,0) = 2 \cdot \sigma(\frac{1}{\sqrt{2}}\,x) \; , \quad G^-(x,0) \;=\; 0 \; , \tag{10}$$

$$\partial_x G^+(x,y)|_{y=0} = \partial_y G^-(x,y)|_{y=0} \;=\; \sqrt{2} \cdot \sigma'(\frac{1}{\sqrt{2}}\,x) \; , \tag{11}$$

$$\partial_y G^+(x,y)|_{y=0} = \partial_x G^-(x,y)|_{y=0} \;=\; 0 \; , \tag{12}$$

where $\sigma'(x) = \sigma(x)(1-\sigma(x))$ denotes the derivative of the sigmoid (2). According to lemma 1 every orbit of $\tilde{F}_\rho$ through a synchronized state $(\xi, 0) \in M$ is constrained to M for all times. With $s := 1/\sqrt{2}\,\xi$, the corresponding synchronized n-dimensional dynamics F^s_ρ in M is described by the Eqs.

$$s_i(t+1) = \theta_i + \sum_{j=1}^{n} w^+_{ij} \cdot \sigma(s_j(t)) \; , \quad i = 1, \ldots, n \; . \tag{13}$$

This Eq. demonstrates that the synchronized dynamics F^s_ρ in M reproduces the dynamics of a single isolated n-module with connectivity matrix w^+. This means that the synchronized dynamics in M may have fixed point attractors as well as periodic, quasiperiodic or chaotic attractors. There may even be co-existing attractors in the synchronization manifold M. From Eq. (13) we can also read that different types of coupling n-modules may produce qualitatively different dynamical effects. If

$$w_{ij} \neq 0 \; , \quad w^{coup}_{ij} \neq 0 \; , \quad \text{and} \quad \text{sign}(w_{ij}) = \text{sign}(w^{coup}_{ij}) \; ,$$

for some index pairs (ij), then the synchronized dynamics of the coupled system comprises more or less the same dynamical properties as the initial isolated n-module. But if the sign of a coupling w^{coup}_{ij} is different from the sign of the corresponding w_{ij} and if it is strong enough, then the synchronized dynamics may differ qualitatively from the dynamics of the isolated module. This is, for instance, the case if loop properties of the module, being even or odd, are changed. Recall, that a loop is termed even (odd) if the number of inhibitory connections in the loop is even (odd). This second condition reads

$$w_{ij} \neq 0 \; , \quad w^{coup}_{ij} \neq 0 \; , \quad \text{and} \quad w_{ij} \cdot w^{coup}_{ij} < -\,(w_{ij})^2 \; ,$$

for some index pairs (ij). An interesting situation may occur if the coupling 'introduces' a new connection in the module architecture, i.e. if

$$w_{ij} = 0 \ , \quad \text{and} \quad w_{ij}^{coup} \neq 0 \ ,$$

for some index pairs (ij). Then properties of the synchronized dynamics may be totally different from those of the isolated n-modules. Examples of these situations are given in the following.

Although the persistence of the synchronized dynamics (13) is guaranteed by conditions (5) and (6), it is not at all clear that the synchronization manifold M is itself asymptotically stable with respect to the dynamics $\tilde{F}_\rho$. Thus, a periodic or chaotic orbit in M may be an attractor for the synchronized dynamics F_ρ^s but not for the dynamics $\tilde{F}_\rho$ of the coupled system. To discuss the stability aspects of the synchronization manifold M it is effective to consider the *synchronization exponents* λ_i^s and the *transversal exponents* $\lambda_i^\perp$, $i = 1, \ldots, n$ for the synchronized dynamics (13). They are derived from the linearization $D\tilde{F}_\rho(s)$ of $\tilde{F}_\rho$ around synchronized states $s(t) = \frac{1}{\sqrt{2}} \cdot \xi(t)$. Using the properties (10) of the functions $G^\pm$ we have

$$D\tilde{F}_\rho(s) = \begin{pmatrix} L^+(s) & 0 \\ 0 & L^-(s) \end{pmatrix} \ , \tag{14}$$

$$L_{ij}^\pm(s) := w_{ij}^\pm \cdot \sigma'(s_j) \ , \quad i, j = 1, \ldots, n \ . \tag{15}$$

The Lyapunov exponents λ_i^s and $\lambda_i^\perp$ are then derived from the eigenvalues of the matrix $L^+(s)$ and $L^-(s)$, as usual.

Synchronized chaotic dynamics will be characterized by a situation where the largest synchronization exponent λ_1^s is positive; i.e. $\lambda_1^s > 0$. On the other hand, an unstable synchronization manifold M will be characterized by a largest transversal exponent $\lambda_1^\perp(s)$ - with respect to a synchronized orbit - satisfying $\lambda_1^\perp > 0$. Thus, if a stable manifold M, containing a chaotic orbit, will turn unstable, then the coupled system will enter a hyperchaotic regime, [Rössler, 1979]; i.e. at least two Lyapunov exponents of the system are positive.

For identical modules with symmetric couplings it makes sense to introduce the point-reflection operator $\mathbf{S}^\eta$ acting only on the η-coordinates of the (ξ, η)-phase space, i.e.

$$\mathbf{S}^\eta(\xi, \eta) = (\xi, -\eta) \ .$$

The functions G^+ and G^- defined in (9) have the property

$$G^+ \ \mathbf{S}^\eta(\xi_i, \eta_i) = G^+(\xi_i, \eta_i) \ , \quad G^- \ \mathbf{S}^\eta(\xi_i, \eta_i) = -G^-(\xi_i, \eta_i) \ , \quad i = 1, \ldots, n \ .$$

Thus the dynamics $\tilde{F}_\rho : \mathbf{R}^{2n} \to \mathbf{R}^{2n}$ given by Eq. (7) is equivariant under the action of $\mathbf{S}^\eta$; i.e.

$$\tilde{F}_\rho \, (\xi, \eta) = (\mathbf{S}^\eta)^{-1} \, \tilde{F}_\rho \, \mathbf{S}^\eta(\xi, \eta) \ .$$

As a consequence of this equivariance property we obtain the following

Lemma 2 *Let $\tilde{F}_\rho$ denote the dynamics (7) of two symmetrically coupled identical n-modules, and let F_ρ^p denote its p-fold iterate. For a point $(\xi, \eta) \in \mathbf{R}^{2n}$ we then have*

$$(\xi, \eta) = \tilde{F}_\rho^p\,(\xi, \eta) \quad \Longleftrightarrow \quad (\xi, -\eta) = \tilde{F}_\rho^p\,(\xi, -\eta)\ .$$

The fact that with (ξ, η) also $(\xi, -\eta)$ must be a p-periodic point does of course *not* include that both points belong to the same p-periodic orbit. As a trivial consequence of lemma 2 we have

Corollary 1 *Let $\tilde{F}_\rho$ denote the dynamics of two coupled identical neurons. If (ξ, η) and $(\xi, -\eta)$ belong to the same period-p orbit of $\tilde{F}_\rho$ then $p = 2q$, and $(\xi, -\eta) = \tilde{F}_\rho^q(\xi, \eta)$.*

For a characterization of attractors in coupled neuromodules the following definition is useful [Abraham *et al.*, 1997]: A quasiperiodic or chaotic attractor is called *p-cyclic* if it has p connected components which are permuted cyclically by the map $\tilde{F}_\rho$. Every component of a p-cyclic attractor is an attractor of $\tilde{F}_\rho^p$. We then may generalize lemma 1 to

Lemma 3 *Let $\tilde{F}_\rho$ denote the dynamics (7) of two symmetrically coupled identical n-modules. If a point $(\xi, \eta) \in \mathbf{R}^{2n}$ lies on a p-cyclic attractor, then also $(\xi, -\eta)$ lies on a, not necessarily the same, p-cyclic attractor.*

3 Examples: Symmetrically coupled 2-Modules

We will discuss two simple examples of coupled neuromodules, each module consisting only of two neurons. The architecture of the two coupled systems is shown in Fig. 1. The first example (Fig. 1, left) considers the coupling of two identical chaotic modules, where, for certain parameter values, the synchronized dynamics is also chaotic. The second situation (Fig. 1, right) describes the coupling of two oscillatory modules, resulting in an (unstable) synchronized dynamics.

3.1 Example 1: Coupled chaotic 2-modules

In this subsection we consider a 2-neuron module consisting of an excitatory unit bi-directionally coupled to an inhibitory unit with self-connection. It is the minimal network configuration with standard graded neurons allowing for discrete chaotic dynamics. This module dynamics is given by a five parameter family of maps $f_\rho : \mathbf{R}^2 \to \mathbf{R}^2$, $\rho = (\theta_1, w_{12}, \theta_2, w_{21}, w_{22}) \in \mathbf{R}^5$, defined by

$$a_1(t+1) \;:=\; \theta_1 + w_{12}\,\sigma(a_2(t))\ , \tag{16}$$

$$a_2(t+1) \;:=\; \theta_2 + w_{21}\,\sigma(a_1(t)) + w_{22}\,\sigma(a_2(t))\ . \tag{17}$$

This module has a large parameter domain, where its dynamics has a global chaotic attractor, but also the coexistence of periodic and chaotic attractors are

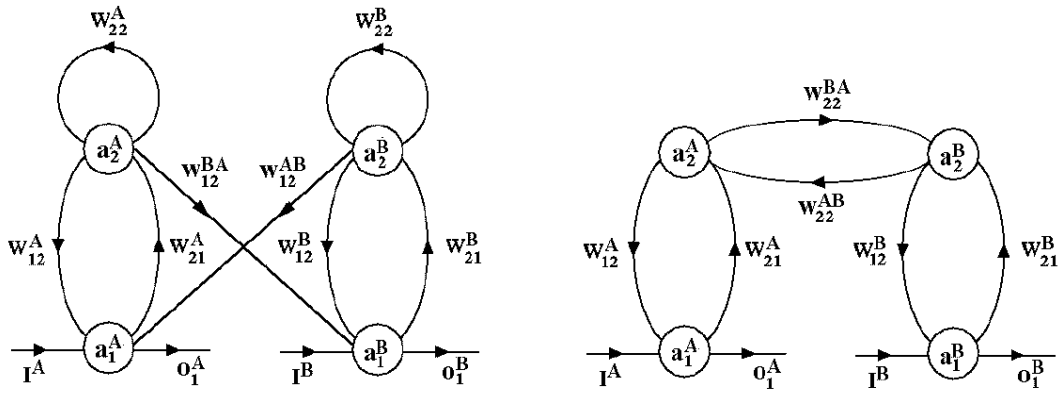

Figure 1: Coupling of 2-neuron modules: chaotic modules (left) and oscillatory modules (right).

observed [Pasemann, 1995a]. We will now couple two of such modules (16) having identical parameter sets $\rho = \rho^A = \rho^B$. There are of course many ways to couple the chaotic 2-modules. At first we will consider inhibitory couplings from the inhibitory neuron of a module to the excitatory neuron of the other module as shown in Fig. 1. The corresponding 4-dimensional dynamics F_ρ of the coupled identical 2-modules A and B is given by

$$\begin{aligned} a_1(t+1) &= \theta_1^A + w_{12}^A\,\sigma(a_2(t)) + w_{12}^{AB}\,\sigma(b_2(t)) \quad , \\ a_2(t+1) &= \theta_2^A + w_{21}^A\,\sigma(a_1(t)) + w_{22}^A\,\sigma(a_2(t)) \quad , \\ b_1(t+1) &= \theta_1^B + w_{12}^B\,\sigma(b_2(t)) + w_{12}^{BA}\,\sigma(a_2(t)) \quad , \\ b_2(t+1) &= \theta_2^B + w_{21}^B\,\sigma(b_1(t)) + w_{22}^B\,\sigma(b_2(t)) \quad . \end{aligned} \tag{18}$$

For simplicity, we will choose parameters $\rho = (\theta, w, w^{coup})$ satisfying condition (6), and we fix connections $-w_{12} = w_{21} = 6$, $w_{22} = -16$, so that the modules can operate in a chaotic mode. Switching to the (ξ, η)-coordinates introduced by Eq. (4), the linearization (14) of the corresponding dynamics $\tilde{F}_\rho$ at synchronized states s is given by the matrices $L^\pm$ defined by equation (15); here we have

$$L^+ = \begin{pmatrix} 0 & (w_{12} + w_{12}^{coup})\,\sigma'(s_2) \\ w_{21}\,\sigma'(s_1) & w_{22}\,\sigma'(s_2) \end{pmatrix} , \tag{19}$$

$$L^- = \begin{pmatrix} 0 & (w_{12} - w_{12}^{coup})\,\sigma'(s_2) \\ w_{21}\,\sigma'(s_1) & w_{22}\,\sigma'(s_2) \end{pmatrix} . \tag{20}$$

3.1.1 Numerical results

Simulations reveal that stable synchronization of coupled identical 2-modules can be achieved over a large range of parameter values, and it is found for periodic as well as for chaotic dynamics. This is shown, for instance, for fixed parameters $\theta_2 =$

-1, $-w_{12} = w_{21} = 6$, $w_{22} = -16$, $w_{12}^{coup} = -3$, and varying θ_1 in Fig. 2, where the largest synchronization and transversal exponents, λ_1^s and $\lambda_1^\perp$, respectively, are depicted. These Lyapunov exponents correspond to the bifurcation diagram for the synchronized dynamics with respect to θ_1 shown in Fig. (3). Starting with a quasi-periodic orbit at zero, and after a larger period-4 window, there are various bifurcation sequences to chaos following the period-doubling route. This can be read also from the corresponding synchronization exponent λ_1^s in Fig. (2). There we see θ_1-intervals, for which the transversal exponent $\lambda_1^\perp$ is positive; i.e. the corresponding synchronized dynamics on M is unstable. The underlying data file locates larger intervals as $(0.0, 0.5)$, $(3.18, 3.58)$, $(5.36, 6.08)$. Thus, already the synchronized quasi-periodic dynamics in the interval $(0.0, 0.5)$ is unstable. The second interval $(3.18, 3.58)$ corresponds to a rare situation where the *unstable* synchronization manifold M contains only *periodic* synchronized orbits.

Fixing module parameters in the chaotic domain, it is in general observed that stable synchronization domains for identical module inputs/bias terms θ_1 are larger for stronger inhibitory couplings; i.e., for growing inhibitory couplings w_{12}^{coup} the transversal Lyapunov exponents are getting smaller. An example is shown in Fig. (5) for fixed parameters $\theta_1 = 6$, $\theta_2 = -2$, $-w_{12} = w_{21} = 6$, $w_{22} = -16$, and varying w_{12}^{coup}. There are now different possibilities for de-synchronization of the modules. According to lemma 1, identical modules de-synchronize immediately after the external input signals θ_1 and/or θ_2 diverge. A second method is to destabilize the synchronization manifold M without violating the synchronization condition (5). This may be done by varying one of the other four parameters. For instance, one may vary the identical external inputs θ_2 to the inhibitory units; this will destabilize the synchronization manifold M in larger domains as can be read from the largest transversal Lyapunov exponent shown in Fig. 6 for fixed parameters $\theta_1 = 6$, $-w_{12} = w_{21} = 6$, $w_{22} = -16$, $w_{12}^{coup} = -3$, and varying θ_2. Thus, keeping the inputs θ_1 to the excitatory units fixed, and varying only the inputs θ_2 to the inhibitory units will drive the coupled system through different de-synchronization regions. Here they correspond to θ_2-intervals $(-4.56, -4.02)$, $(-3.72, -2.66)$, $(-2.08, -1.58)$, as can be read from the underlying data file.

So far we have only considered the synchronized dynamics constrained to the synchronization manifold M. But the following observation is noteworthy as well: For large parameter domains stable synchronized dynamics can co-exist with asynchronous periodic, quasi-periodic or chaotic attractors not constrained to M. In Fig. (4) a whole bifurcation sequence with respect to varying θ_1 for the asynchronous dynamics is depicted. All these attractors co-exist with the synchronized orbits of Fig. (3). In fact, for some values of θ_1 there are even more than two co-exiting attractors: Co-existence of synchronous and asynchronous attractors is demonstrated, for instance, in Figs. 7 and 8, where a synchronized chaotic attractor co-exists with asynchronous period-2 and 2-cyclic chaotic attractors, respectively. In Fig. 9 a 2-cyclic hyperchaotic attractor surrounding the unstable synchronization manifold M is depicted which co-exists with an asyn-

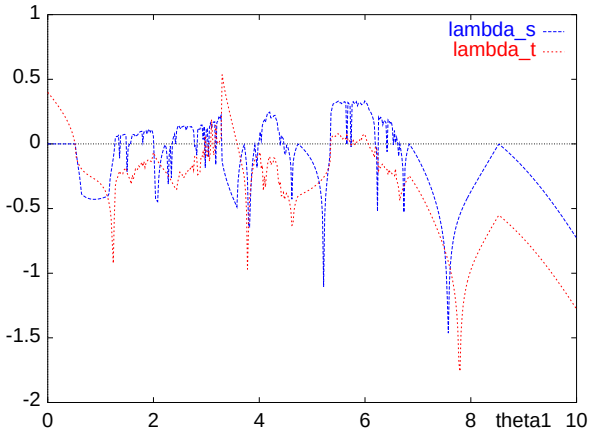

Figure 2: Largest synchronization and transversal exponents for fixed parameters $\theta_2 = -1$, $-w_{12} = w_{21} = 6$, $w_{22} = -16$, $w_{12}^{coup} = -3$, and varying θ_1.

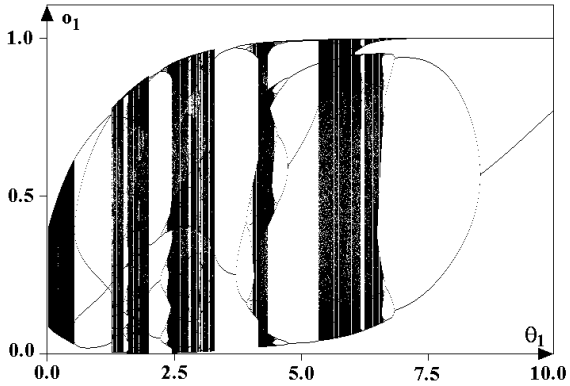

Figure 3: Bifurcation diagram of the synchronized dynamics for the same parameter values as in Fig. 2.

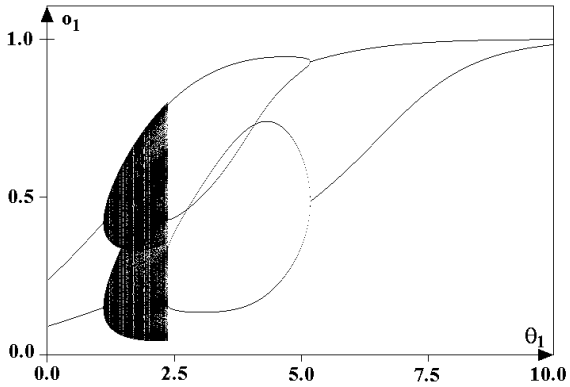

Figure 4: Bifurcation diagram of an asynchronous dynamics for the same parameter values as in Fig. 2.

chronous period-2 orbit. In these Figs. the projections of co-existing attractors onto the (o_1^A, o_2^A)-phase space of module A (left Figs.) and onto the (o_1^A, o_1^B)-output space of the coupled system (right Figs.) is shown. Synchronized outputs will appear as states lying on the main diagonal in (o_1^A, o_1^B)-space. The parameters for these configurations can be found in the figure legends. Furthermore,

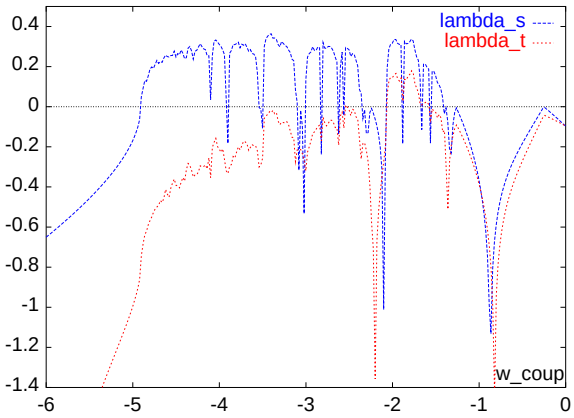

Figure 5: Largest synchronization and transversal exponents for fixed parameters $\theta_1 = 6$, $\theta_2 = -2$, $-w_{12} = w_{21} = 6$, $w_{22} = -16$, and varying w_{12}^{coup}.

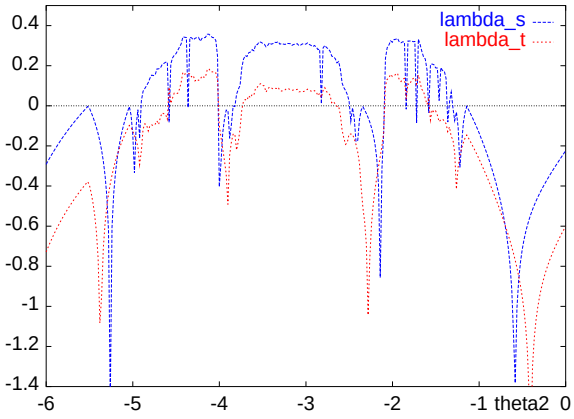

Figure 6: Largest synchronization and transversal exponents for fixed parameters: $\theta_1 = 6$, $-w_{12} = w_{21} = 6$, $w_{22} = -16$, $w_{12}^{coup} = -2$ and varying θ_2.

we can find also different co-existing attractors constrained to the stable synchronization manifold M. For the fixed parameters $\theta_2 = -2.5$, $-w_{12} = w_{21} = 6$, $w_{22} = -16$, $w_{12}^{coup} = -3$, and $\theta_1 = 0.4$, we observe a synchronous period-3 and a synchronous quasiperiodic attractor co-existing with an asynchronous period-2 attractor. For $\theta_1 = 3.67$ we find a period-3 attractor and a chaotic attractor, both constrained to the synchronization manifold M. No Figs. are shown for these examples.

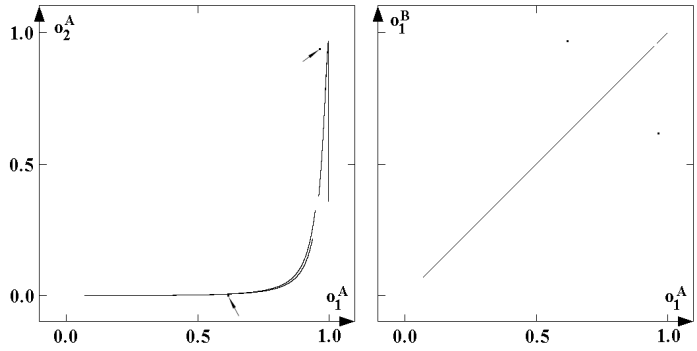

Figure 7: A synchronized 2-cyclic chaotic attractor co-existing with an asynchronous period-2 attractor. Projections to module space (left) and to the output space of the coupled system (right). Parameters: $\theta_1 = 6.1$, $\theta_2 = -1$, $-w_{12} = w_{21} = 6$, $w_{22} = -16$, $w_{12}^{coup} = -3$.

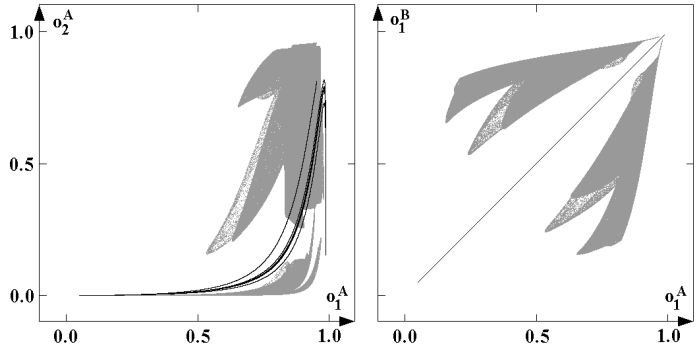

Figure 8: A synchronized chaotic attractor constrained to M co-exists with an asynchronous 2-cyclic chaotic attractor. Parameters: $\theta_1 = 4.4$, $\theta_2 = -2$, $-w_{12} = w_{21} = 6$, $w_{22} = -16$, $w_{12}^{coup} = -3$.

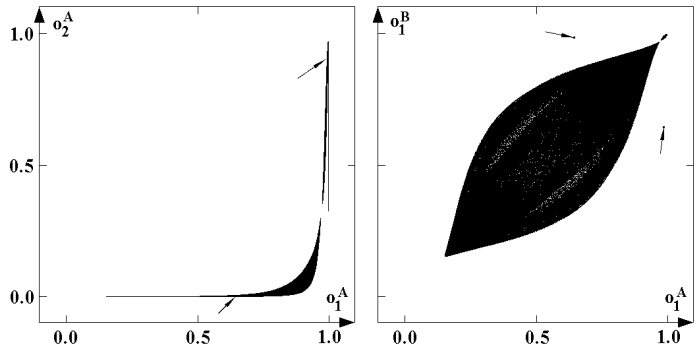

Figure 9: A 2-cyclic hyperchaotic attractor surrounding the unstable synchronization manifold M. It co-exists with an asynchronous period-2 attractor. Parameters: $\theta_1 = 6.0$, $\theta_2 = -1.65$, $-w_{12} = w_{21} = 6$, $w_{22} = -16$, $w_{12}^{coup} = -2$.

3.2 Example 2: Coupled oscillatory 2-modules

The first example showed that coupling of chaotic modules can result in stable synchronized dynamics. For the second example we will consider modules consisting of interacting excitatory and inhibitory units without self-connections. For all parameter values they have only fixed point or period-4 attractors [Pasemann, 1995b]. We will consider couplings between the inhibitory units to observe complex dynamics in the composed system

$$\begin{aligned} a_1(t+1) &= \theta_1^A + w_{12}^A\,\sigma(a_2(t))\;, \\ a_2(t+1) &= \theta_2^A + w_{21}^A\,\sigma(a_1(t)) + w_{22}^{AB}\,\sigma(b_2(t))\;, \\ b_1(t+1) &= \theta_1^B + w_{12}^B\,\sigma(b_2(t))\;, \\ b_2(t+1) &= \theta_2^B + w_{21}^B\,\sigma(b_1(t)) + w_{22}^{BA}\,\sigma(a_2(t))\;. \end{aligned} \tag{21}$$

Again, we will choose parameters $\rho = (\theta, w, w^{coup})$ satisfying condition (6), and we will fix weights by $-w_{12} = w_{21} = 6$. The synchronized dynamics (13) for this setup reads

$$\begin{aligned} s_1(t+1) &= \theta_1 + w_{12}\,\sigma(s_2(t))\;, \\ s_2(t+1) &= \theta_2 + w_{21}\,\sigma(s_1(t)) + w_{22}^{coup}\,\sigma(s_2(t))\;, \end{aligned} \tag{22}$$

and it corresponds to the dynamics of an isolated chaotic module (16) used as basic module in example 1 above. Thus, the range of dynamical behaviors of the synchronized dynamics exceeds that of an isolated module by far. To consider stability properties of this synchronized dynamics we study the linearization (14) of the (ξ, η)-dynamics $\tilde{F}_\rho$ given by (4). In terms of matrices $L^\pm$ it has the form

$$L^+ = \begin{pmatrix} 0 & w_{12}\,\sigma'(s_2) \\ w_{21}\,\sigma'(s_1) & w_{22}^{coup}\,\sigma'(s_2) \end{pmatrix}\;, \tag{23}$$

$$L^- = \begin{pmatrix} 0 & w_{12}\,\sigma'(s_2) \\ w_{21}\,\sigma'(s_1) & -w_{22}^{coup}\,\sigma'(s_2) \end{pmatrix}\;. \tag{24}$$

From this we read immediately that the eigenvalues $\epsilon^s(s)$ and $\epsilon^\perp(s)$ of the matrices $L^+(s)$ and $L^-(s)$, respectively, satisfy

$$|\epsilon^s(s)| = |\epsilon^\perp(s)|\;, \quad s \in \mathbf{R}\;,$$

and it follows that the largest synchronization exponent is equal to the largest transversal exponent; i.e.

$$\lambda_1^s = \lambda_1^\perp\;. \tag{25}$$

Although this coupled system allows synchronized chaos, it will never be stable because of (25); i.e., if the system is chaotic it will always be hyperchaotic.

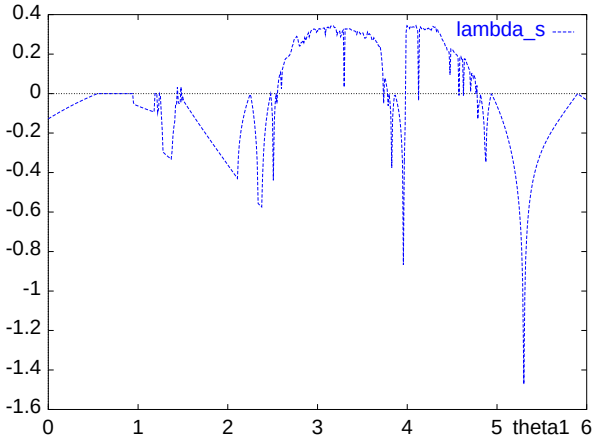

Figure 10: Largest synchronization and transversal exponents $\lambda_1^s = \lambda_1^\perp$ for fixed parameters $\theta_2 = -2.5$, $-w_{12} = w_{21} = 6$, $w_{22}^{coup} = -16$, and varying θ_1.

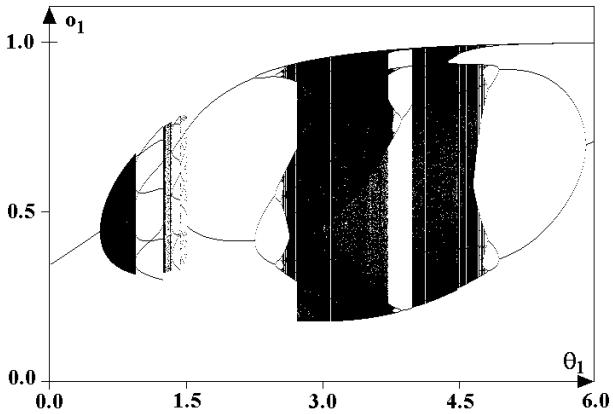

Figure 11: Bifurcation diagram of the synchronized dynamics for the same parameter values as in Fig. 10.

3.2.1 Numerical results

Simulation were done for fixed parameters $\theta_2 = -2.5$, $-w_{12} = w_{21} = 6$, and $w_{22}^{coup} = -16$. In Fig. 10 the two identical Lyapunov exponents $\lambda_1^s = \lambda_1^\perp$ are depicted for varying θ_1. They correspond to the bifurcation diagram of the synchronized dynamics, which is shown in Fig. 11. After a bifurcation from a fixed point attractor to a synchronized quasiperiodic orbit there follows a domain with different periodic attractors, and, starting from a larger interval of period-2 attractors, a typical period-doubling route to chaos finally ends again with a period-2 attractor at $\theta_1 = 6$.

The dynamics of the coupled two modules (21) corresponds of course to that of a bidirectional chain with two odd loops at the ends and an even loop in the middle. For all parameter values, i.e. also for small w_{22}^{coup}, the dynamics appears

as that of two *isolated* modules with their inhibitory units having an inhibitory self-connection. This can be observed, for instance, by projecting the attractors on the (o_1^A, o_1^B)-subspace as in Fig. 12. As can be read from the bifurcation diagram for the synchronous dynamics in Fig. 11, for $\theta_1 = 0.9$ the modules have a quasiperiodic attractor and the manifold M is neutral (i.e. $\lambda_1^{\perp} = 0$). Although there is a quasiperiodic orbit constrained to M, depending on the initial conditions the orbits will lie on a 2-dimensional torus in $\mathbf{R}^4$. Projecting these orbits into the subspaces will result in a dense set of orbits in the projection space. Three of such orbits are shown in Fig. 12 (left). The right part of the same Fig. shows a 2-cyclic hyperchaotic attractor placed symmetrically around the synchronization manifold M, and two co-existing 1-cyclic chaotic attractors for $\theta_1 = 2.7$. They are generated as follows: Each (quasi-isolated) module has a 2-cyclic chaotic attractor corresponding to the (unstable) synchronous dynamics of the coupled system. Depending on initial conditions, the orbit may start in the same part of the attractor - resulting in the 2-cyclic chaotic attractor (black) symmetric to the manifold M - or in different parts, which gives the two other 1-cyclic chaotic attractors. Not shown is the situation for e.g. $\theta_1 = 0.95$, where the stable synchronized dynamics has a period-7 attractor. In the coupled system periodic points lie on a 7×7 quadratic grid corresponding to three asynchronous period-14 orbits and one period-7 orbit constrained to the synchronization manifold M. Thus, all these examples display the dynamics of two isolated neuromodules, each having dynamical properties corresponding to the synchronized dynamics of the coupled systems. Furthermore, simulations suggest that the same holds true also for couplings $|w_{22}^{coup}| < |w12|$.

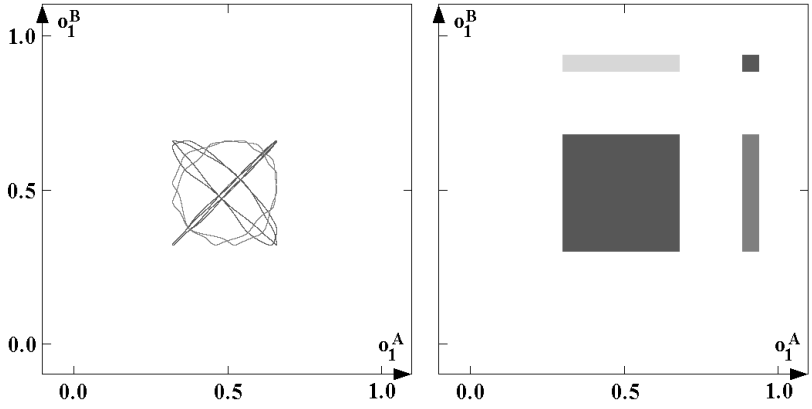

Figure 12: Projections onto (o_1^A, o_1^B)-space: Quasiperiodic attractors (left, $\theta_1 = 0.9$), and a 2-cyclic chaotic attractor co-existing with two 1-cyclic chaotic attractors (right, $\theta_1 = 2.7$) for parameters $\theta_2 = -2.5$, $-w_{12} = w_{21} = 6$, $w_{22} = 0$, $w_{22}^{coup} = -16$ (see text for details).

4 Conclusions

It has been shown that in certain systems of two coupled neuromodules synchronized chaos as well as synchronized periodic or quasiperiodic dynamics can exist. Modules of the composed system had the same number of neurons and identical architectures. All conditions for the existence of synchronized dynamics required that the sum of bias terms and stationary external inputs to corresponding module neurons are identical. Depending on module parameters, orbits constrained to a synchronization manifold can be globally or locally stable, or unstable. For large parameter domains stable synchronous dynamics will co-exist with asynchronous periodic, quasiperiodic or even chaotic attractors. Thus, whether a system ends up asymptotically in a synchronous mode or not depends crucially on initial conditions, i.e. on the internal state of the system. In this sense the reaction to external signals depends also on the *history* of the system itself. This may introduce *memory effects* into the behavior of coupled systems. Furthermore, a synchronized mode often persists even if external inputs are varying slowly. Thus, synchronization of coupled modules is really a sign for time-varying (identical) input signals with amplitudes having a *fixed ratio* (recall, that the inputs may correspond to the weighted outputs of other neurons in a larger system).

De-synchronization of module dynamics can be achieved in different ways. From the synchronization condition (5) it is clear that diverging external inputs or other diverging parameters (like module weights or coupling strengths) will immediately de-synchronize the modules. Different from this standard situation, specific external signals may be used to drive the composed system into unstable synchronization domains. For instance, keeping the identical inputs to excitatory module units fixed and varying the identical inputs to the inhibitory units can drive the system into the unstable synchronization domain (cf. Fig. 6). If one comprehends excitatory neurons as signal processing units, and inhibitory neurons as concerned with local computations - a common interpretation in the context of biological neural networks - then synchronization as response to external stimuli may depend on *attention related signals* to inhibitory neurons.

References

[1] Abraham, R. H., Gardini, L., and Mira, C. (1997) *Chaos in Discrete Dynamical Systems*, Springer-Verlag, New York.

[2] Ashwin, P., Buescu, J., and Stewart, I. (1996) From attractor to chaotic saddle: a tale of transverse instability, *Nonlinearity*, **9**, 703–737.

[3] Astakhov, V., Hasler, M., Kapitaniak, T., Shabunin, A., and Anishchenko, V. (1998) Effect of parameter mismatch on the mechanism of chaos synchronization loss in coupled systems, *Phys. Rev. E*, **58**, 5620–5628.

[4] Blum, E. K., and Wang, X. (1992) Stability of fixed points and periodic orbits and bifurcations in analog neural networks, *Neural Networks*, **5**, 577–587.

[5] Chapeau-Blondeau, F., and Chauvet, G. (1992) Stable, oscillatory, and chaotic regimes in the dynamics of small neural networks with delay, *Neural Networks*, **5**, 735-743.

[6] Carroll, T. L. (1995) Synchronization and complex dynamics in pulse-coupled circuit models of neurons, *Biol. Cybern.*, **73**, 553 –559.

[7] Cuomo, K. M., and Oppenheim, A. V. (1993) Circuit implementation of synchronized chaos with applications to communications, *Phys. Rev. Lett.*, **71**, 65–68.

[8] De Sousa Viera, M., Lichtenberg, A. J., and Liebermann, M. A. (1992) Synchronization of regular and chaotic systems, *Phys. Rev. A*, **46**, 7359–7362.

[9] Eckhorn, R., Bauer, R., Jordan, W., Brosch, M., Kruse, W., Munk, M., and Reitboeck, H. J. (1988) Coherent oscillations: a mechanism for feature linking in the visual cortex, *Biol. Cybern.*, **60**, 121-130.

[10] Engel, A. K., Roelfsema, P. R, Fries, P., Brecht, M., and Singer, W. (1997) Binding and response selection in the temporal domain - a new paradigm for neurobiological research? *Theory in Biosciences*, **116**, 241-266.

[11] Hansel, D., and Sompolinsky H. (1992) Synchronization and computation in a chaotic neural network *Phys. Rev. Lett.*, **68**, 718–721.

[12] Hasler, M., Maistrenko, Y., and Popovych, O. (1998) Simple example of partial synchronization of chaotic systems, *Phys. Rev. E*, **58**, 6843–6846.

[13] Heagy, J. F., Carroll, T. L., and Pecora, L. M., (1994) Synchronous chaos in coupled oscillator systems, *Phys. Rev. E*, **50**, 1874–1885.

[14] Hertz, J., Krogh, A., and Palmer, R.G. (1991) *Introduction to the Theory of Neural Computation*, Redwood City: Addison-Wesley.

[15] Kapitaniak, T., Sekieta, M., and Ogorzalek, M. (1996) Monotone synchronization of chaos. *Int. J. Bif. Chaos*, **6**, 211–217.

[16] Kocarev, L., Shang, A., and Chua, L. O. (1993) A unified method of control and synchronization of chaos, *Int. J. Bif. Chaos*, **3**, 479–483.

[17] Maistrenko, Y., and Kapitaniak, T. (1996) Different types of chaos synchronization in two coupled piecewise linear maps, *Phys. Rev. E*, **54**, 3285–3292.

[18] Parlitz, U., Chua, L. O., Kocarev, L., Halle, K. S., and Shang, A. (1992) Transmission of digital signals by chaotic synchronization, *Int. J. Bif. Chaos*, **2**, 973–977.

[19] Pasemann, F. (1995a) Neuromodules: A dynamical systems approach to brain modelling. In H. Herrmann, E. Pöppel, D. Wolf (Eds.), *Supercomputing in Brain Research - From Tomography to Neural Networks*, (pp. 331–347). Singapore: World Scientific.

[20] Pasemann, F. (1995b) Characteristics of periodic attractors in neural ring networks, *Neural Networks*, **8**, 421-429.

[21] Pecora, L. M., and Carroll, T. L. (1990) Synchronization in chaotic systems, *Phys. Rev. Lett.*, **64**, 821–823.

[22] Pecora, L. M., Heagy, J., and Carroll, T. L. (1994) Synchronization and desynchronization in pulse-coupled relaxation oscillators, *Phys. Lett. A*, **186**, 225–229.

[23] Pikovsky, A. S., Rosenblum, M. G., Osipov, G.V., and Kurth s, J. (1997) Phase synchronization of chaotic oscillators by external driving, *Physica D*, **104**, 219–238.

[24] Rössler, O. (1979) An equation for hyperchaos. *Phys. Lett. A*, **71**, 155-157.

[25] Rosenblum, M. G., Pikovsky, A. S., and Kurths, J. (1996) Phase synchronization of chaotic oscillators, *Phys. Rev. Lett.*, **76**, 1804–1807.

[26] Rulkov, N. F., Sushchik, M. M., Tsimring, L. S., and Abarbanel, H. D. I. (1995) General synchronization of chaos in directionally coupled chaotic systems, *Phys. Rev. E*, **51**, 980–994.

[27] Schweizer, J., Kennedy, M. P., Hasler, M., and Dedieu, H. (1995) Synchronization theorem for a chaotic system. *Int. J. Bif. Chaos*, **5**, 297–302.

[28] Singer, W. (1994) Time as coding space in neocortical processing. In: Buzsáki, G.; Llinás, R.; Singer, W.; Berthoz, A., and Christen, Y. (eds.) *Temporal Coding in the Brain*. Springer, Berlin. pp. 51-80.

[29] Venkataramani, S. C., Hunt, B. R., and Ott, E. (1996) Bubbling transition *Phys. Rev. E*, **54**, 1346–1360.

[30] Wang, X (1991) Period-doublings to chaos in a simple neural network: An analytic proof, *Complex Systems*, **5**, 425-441.

[31] Wennekers, T., and Pasemann, F. (1996) Synchronous chaos in high-dimensional modular neural networks, *Int. J. Bif. Chaos*, **6**, 2055-2067.

[32] Wilson, H. R., and Cowan, J. D. (1972) Excitatory and inhibitory interactions in localized populations of model neurons, *Biophysical Journal*, **12**, 1-24.